Detection, Analysis, and Interpretation of Teleseismic Signals

1. Compressional Phases from the Salmon Event

C. B. ARCHAMBEAU,[1] E. A. FLINN, AND D. G. LAMBERT

Seismic Data Laboratory, Teledyne, Inc.
Alexandria, Virginia

The travel times and amplitude spectrums of first- and later-arrival *P* phases from the Salmon event are computed on the basis of polarization filter outputs. The interpretation of the *P* wave radiation field is made in terms of crust and mantle structure using the first- and later-arrival *P* phases and their amplitude spectrums. The observed seismic field corresponds with that expected from a symmetric, purely compressive source. The essential features of the observed travel times and amplitudes are explained in terms of regional mantle structures. These structures provide first-order fits to the observed data and are characterized by low-velocity zones which terminate with rapid and continuous increases in velocity near depths of 130 km. The velocity structures also show a strong velocity gradient near 330 km. The regional models differ most strongly in the relative extent and magnitude of the velocity decrease in the low-velocity zone.

INTRODUCTION

The study to be described was primarily an attempt to use first- and later-arrival *P* phase travel times and amplitude measurements to obtain basic source and path information. The study is confined to a particular event, but the methods and computational programs to be described are applicable to general seismological studies.

Some general observations concerning the Salmon event and the associated seismic field can be made from a preliminary analysis of the signal from this event. In particular, fundamental-mode Rayleigh waves were identified at 21 stations, in the period range 8 to 40 sec, out to about 2500 km. Higher-mode Rayleigh waves were observed to distances of 3000 km on the continent and at nearly every operative LRSM station. *P* phases were detected at all but one or two continental LRSM stations and at La Paz, Bolivia, at a distance of 5704 km. The long-period Rayleigh wave excitation was not great, as might be expected, and the signal-to-noise ratio was generally quite low, except at the closest pair of stations. In addition, the occurrence of an earthquake in Mexico either complicated or completely masked the Rayleigh waves at some of the western stations. Consequently, the analysis of surface wave radiation was limited to the 14 stations indicated in Figure 1. The surface wave data were, however, used as an aid in the interpretation of the body wave radiation.

It is significant to observe that, as with the Gnome event, no Love wave radiation was observed. This is in contrast to most of the Nevada Test Site (NTS) shots, for example Shoal and Bilby, which produce *SH* surface waves of this type. The NTS is in a tectonically active area, and the medium would normally be prestressed, but Salmon and Gnome were in salt and would not support even a small prestress field. Thus the lack of *SH* radiation from Salmon and Gnome would be consistent with the presence of such radiation from NTS events if tectonic release were involved. The observations are still open to other interpretations, however.

DETECTION AND ANALYSIS OF BODY WAVE *P* PHASES

For detection and isolation purposes, a special filter was used in processing the time series. The filter process is termed 'rectilinear motion detection' and abbreviated to 'Remode.' The basic concepts involved in the design of such

[1] Now at the Division of Geological Sciences, California Institute of Technology, Pasadena, California.

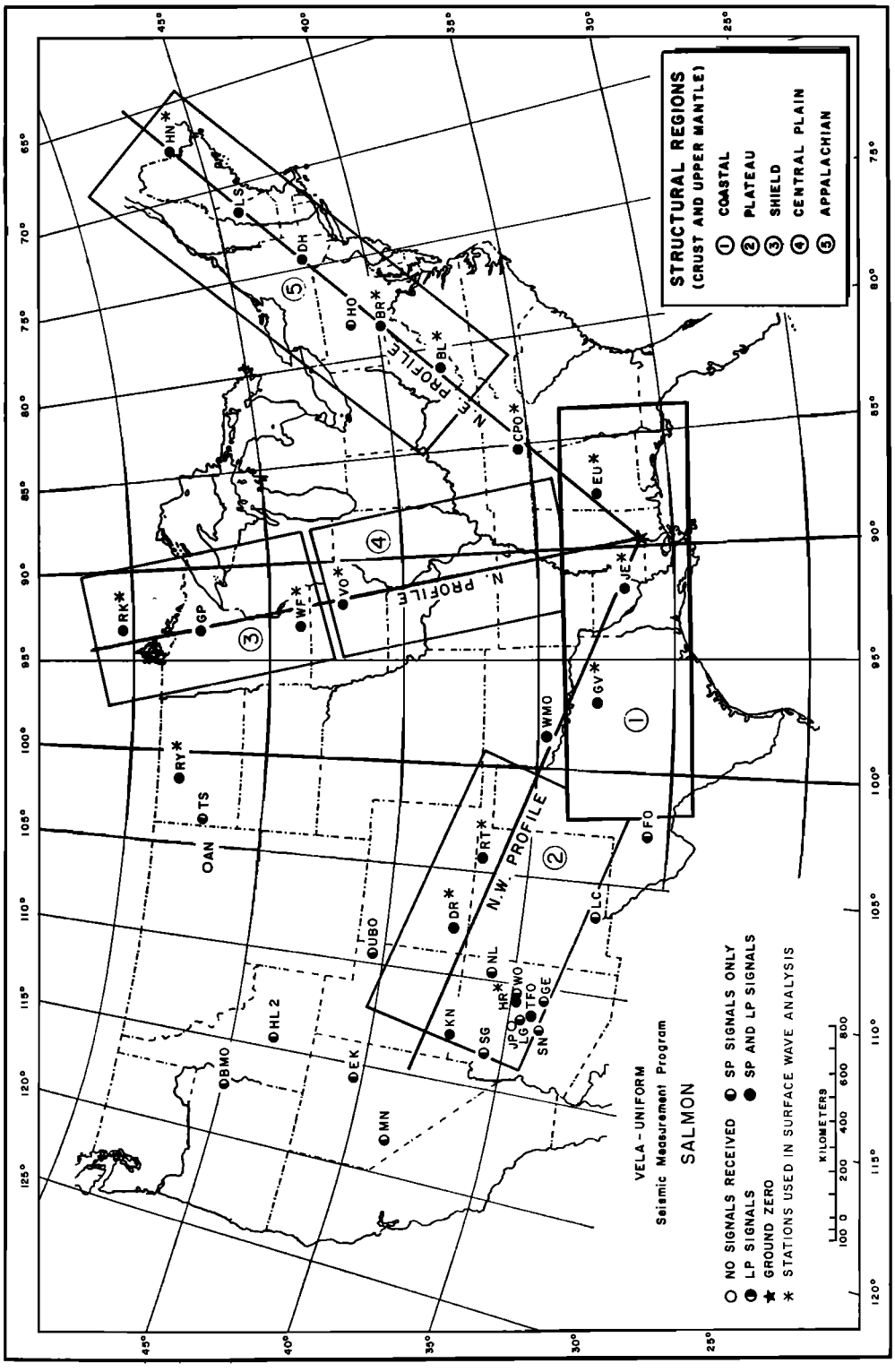

Fig. 1. Station location, signal reception, structural regions, and station-source profiles.

a filter are not new, and several have been successfully used before, most recently by *Shimshoni and Smith* [1964]. In addition, *Sax and Mims* [1965] have described several advanced versions of these filters and investigated some aspects of the theory. The Remode filter used in the present study was developed by the latter authors.

In simplified terms, these filters are designed to pass motion that is rectilinear and to filter out elliptical motion. Thus the motion that is in phase in the radial and vertical directions over a time equal to about 1 cycle of the expected signal is amplified and the motion that is 90° out of phase during this time is attenuated. Such a filter is effective insofar as the noise is predominantly made up of Rayleigh waves and the primary P motion, or initial part of a 'P coda,' is rectilinear. It is assumed that the remainder, or tail of the coda, is superposed P, SV, and Rayleigh motion. These assumptions appear to be valid, at least to a degree, for most of the sites tested.

Analytically, the Remode filter function may be described in terms of the even part of the cross correlation between the radial and vertical components of motion. Such a function, when used as a filter, will selectively attenuate out-of-phase motion on the two traces and will pass in-phase motion. The actual correlation function used is computed over a short time window of width $2T$ centered at a reference time t_0. This correlation function is then used as the filter appropriate to the time t_0. The filter is changed by recomputation of the correlation function as t_0 increases, so that the filter varies with the time t_0. The analytical details are given by *Sax and Mims* [1965] and, for this specific filter, by *Archambeau and Flinn* [1965].

Figure 2 shows two especially good examples of the signal-to-noise enhancement and phase isolation capability of the filter. The event shown is Salmon, and the stations are in the 20° distance range. As might be expected, several clear P arrivals have been isolated and presumably correspond to multiple branches of the travel-time curve.

Of the stations processed in this study, roughly 30% gave outputs with S/N enhancement and phase isolation comparable to the examples shown. The most common failing in the remaining processed records, aside from occasional reductions in the over-all S/N enhancement feature of the process, was the absence of a clearly isolated P_n arrival in the zone where the S/N ratio for P_n was low. This apparent lack of sensitivity may be due to the manner of data presentation (i.e., the scaling of the plotted filter output), but it may indicate a threshold of S/N for detectability—at least with this particular filter. The precise threshold limits are observed to vary from location to location, however, so that one must conclude that the character of the noise and signal, but especially of the noise, determines to a great extent the sensitivity of the filter to small-amplitude rectilinear signals.

Figure 3 indicates the detection sensitivity of the process under what are probably ideal noise conditions. The records shown are from the Oslo, Norway, array at a distance of 7565 km from Salmon, well beyond the range of detection by simple visual or analytical correlation methods. Approximately 4 minutes of record were used from each trace, 2 minutes before and after the predicted P arrival time. Only a section of this time interval is shown in the figure. Before application of the Remode filter none of the array detectors show the signal, nor does the velocity-filtered trace.

Two passes through the filter provide optimum noise reduction and in this case give two arrivals at approximately the times predicted for P and PcP. No other pulse besides these two, or in fact motion of any sort, was observed on the second-pass Remode trace during the 4-minute sample. It seems reasonable to conclude that these pulses result from the arrival of signals from Salmon.

The actual shape of the pulse passed by the filter is likely to be quite distorted, especially when the S/N ratio is low, since, in addition to distortions introduced by the filter itself, the sum of the noise and signal is admitted, inasmuch as the filter acts somewhat like a gate. Hence this filter provides information on the time of first motion and the interval of rectilinearity for a phase but little highly reliable information on the pulse shape. Indeed, one might expect the signal as admitted by a Remode filter to look much like a section of the noise when the S/N ratio is low. This appears to be the case for the Oslo array, although the true shape of the pulse is unknown.

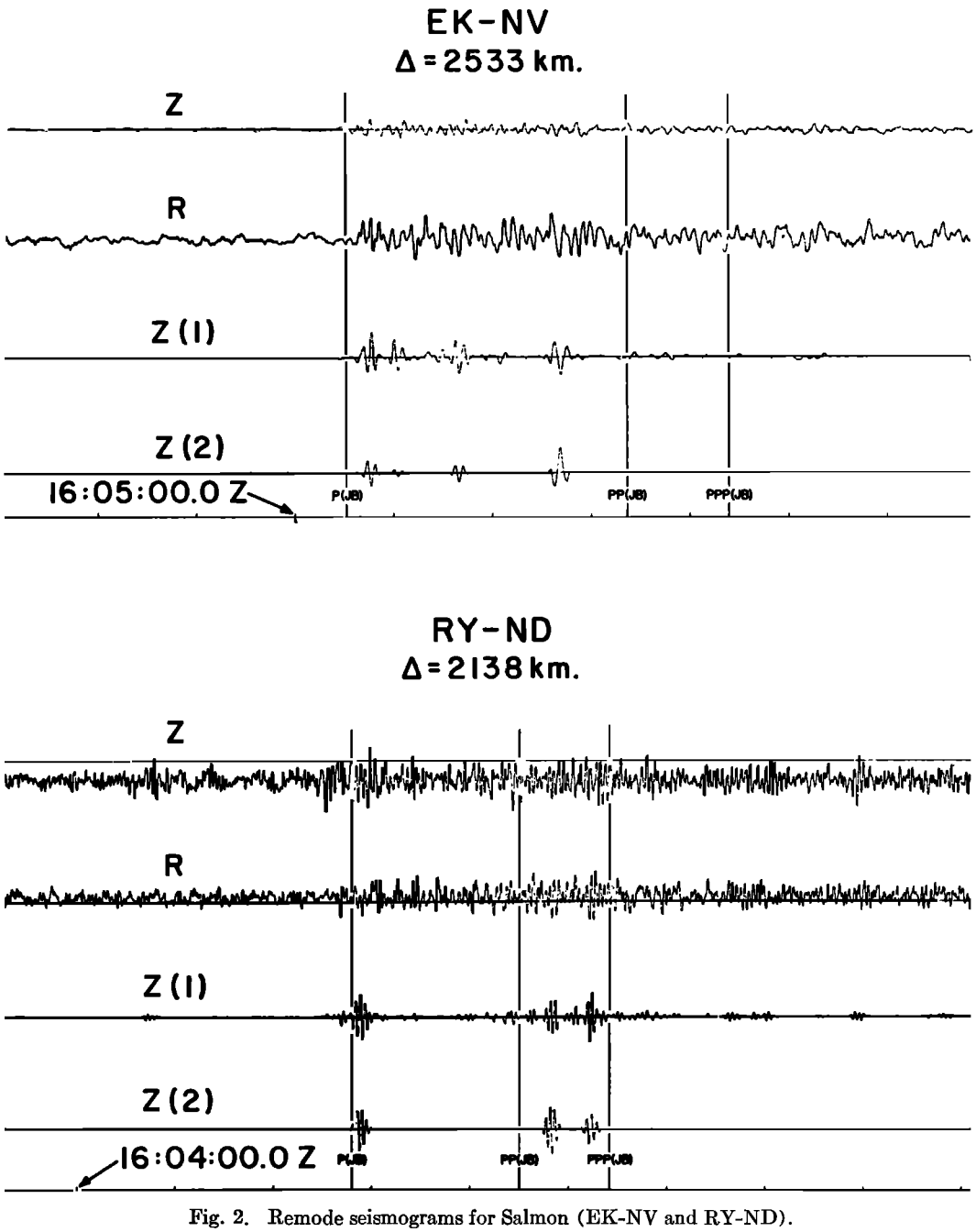

Fig. 2. Remode seismograms for Salmon (EK-NV and RY-ND).

The arrival times and time intervals of rectilinear motion for the phases as indicated by the processed time series were correlated with the original unfiltered records in order to verify the body phases obtained. The travel times of the phases were then plotted as functions of distance along the three profiles indicated in Figure 1. The interval times were used to determine samples of the rectilinear part of the individual arrivals from the unfiltered time

series. Fourier spectrums of the observed first arrivals for all stations along the profile were then computed.

The spectrum and travel-time analyses may be integrated into a single automated analysis program, and Figures 4 and 5 together illustrate the program used to generate these data. The processing entails phase isolation by the Remode process followed by phase identification and velocity filtering of the original time series on the basis of the isolated phases. The spectrums of the various phases are then computed and corrected for instrument response and all preliminary filtering. In addition, as shown in Figure 5, the dispersion of the phases can be measured by subjecting the signals to very narrow, high Q filtering operations at a large number of closely spaced frequencies. The peaks in the envelope of a filtered signal are then determined, and the times of envelope maximums, corrected for instrument group delay, are taken as group arrivals at the center frequency of the filter. Finally, the amplitudes of these envelope maximums are measured. By choosing the maximum of all the envelope maximums at each filter center frequency, we obtain the arrival time as a function of frequency for a particular phase. The amplitudes of the envelope corresponding to these times of arrival then give a relative measure of the amplitude spectrum of the signal, in addition to the Fourier spectrum computed in the usual manner.

Figure 5 shows the envelope maximums as

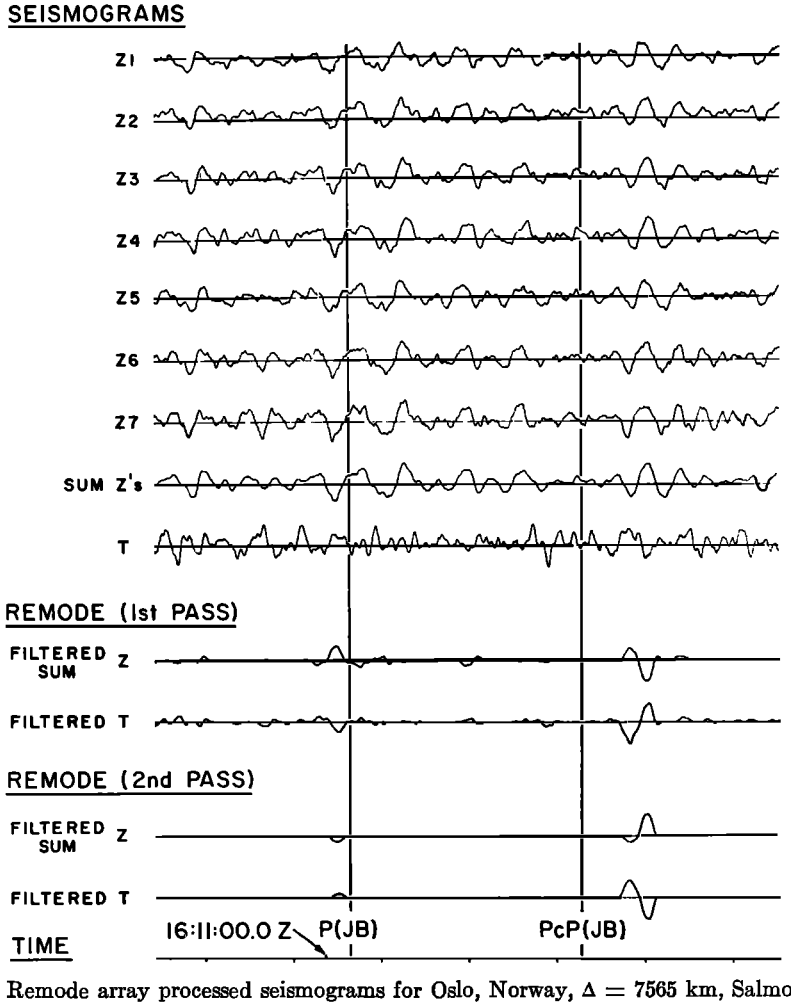

Fig. 3. Remode array processed seismograms for Oslo, Norway, $\Delta = 7565$ km, Salmon event.

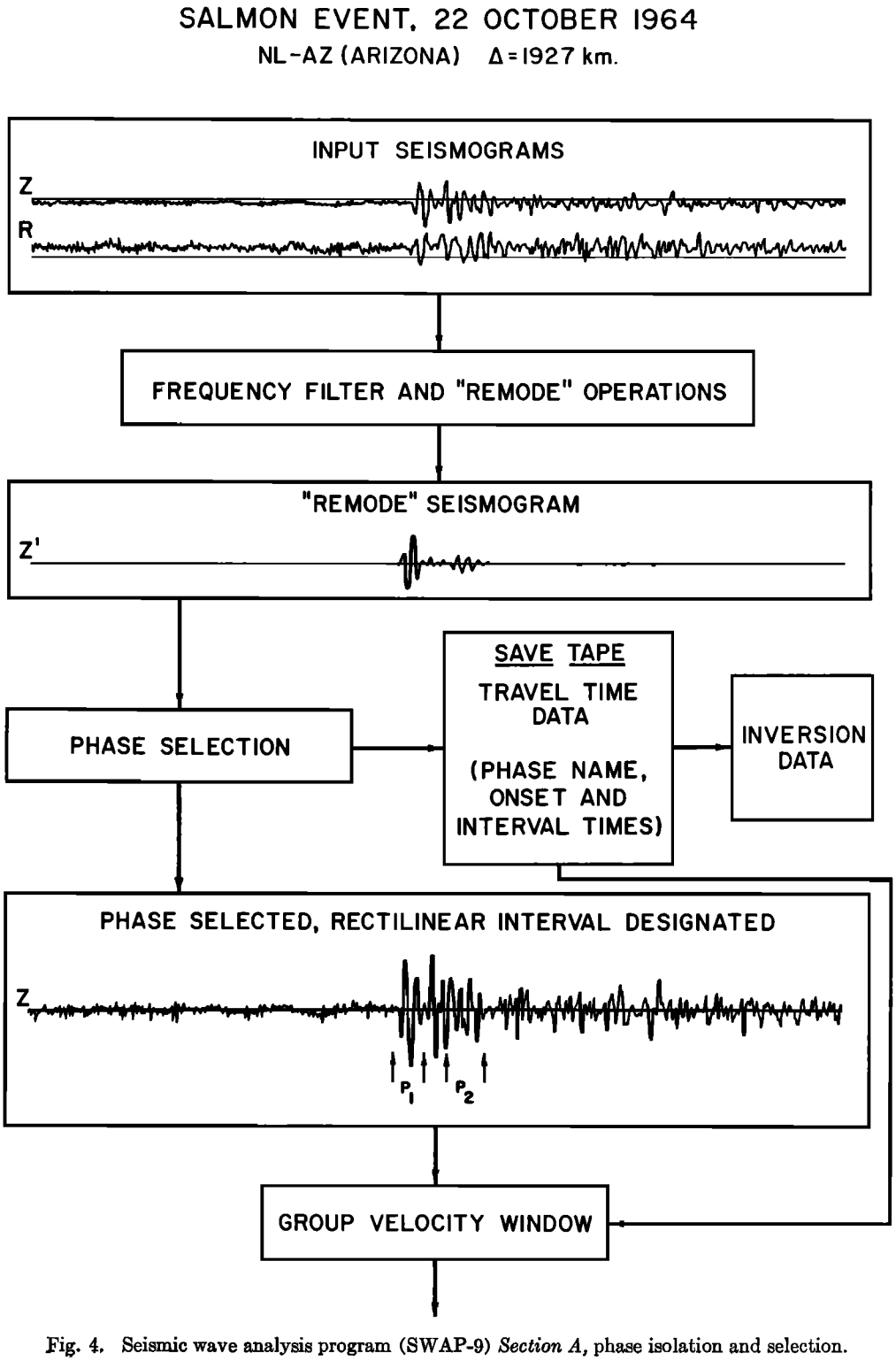

Fig. 4. Seismic wave analysis program (SWAP-9) *Section A*, phase isolation and selection.

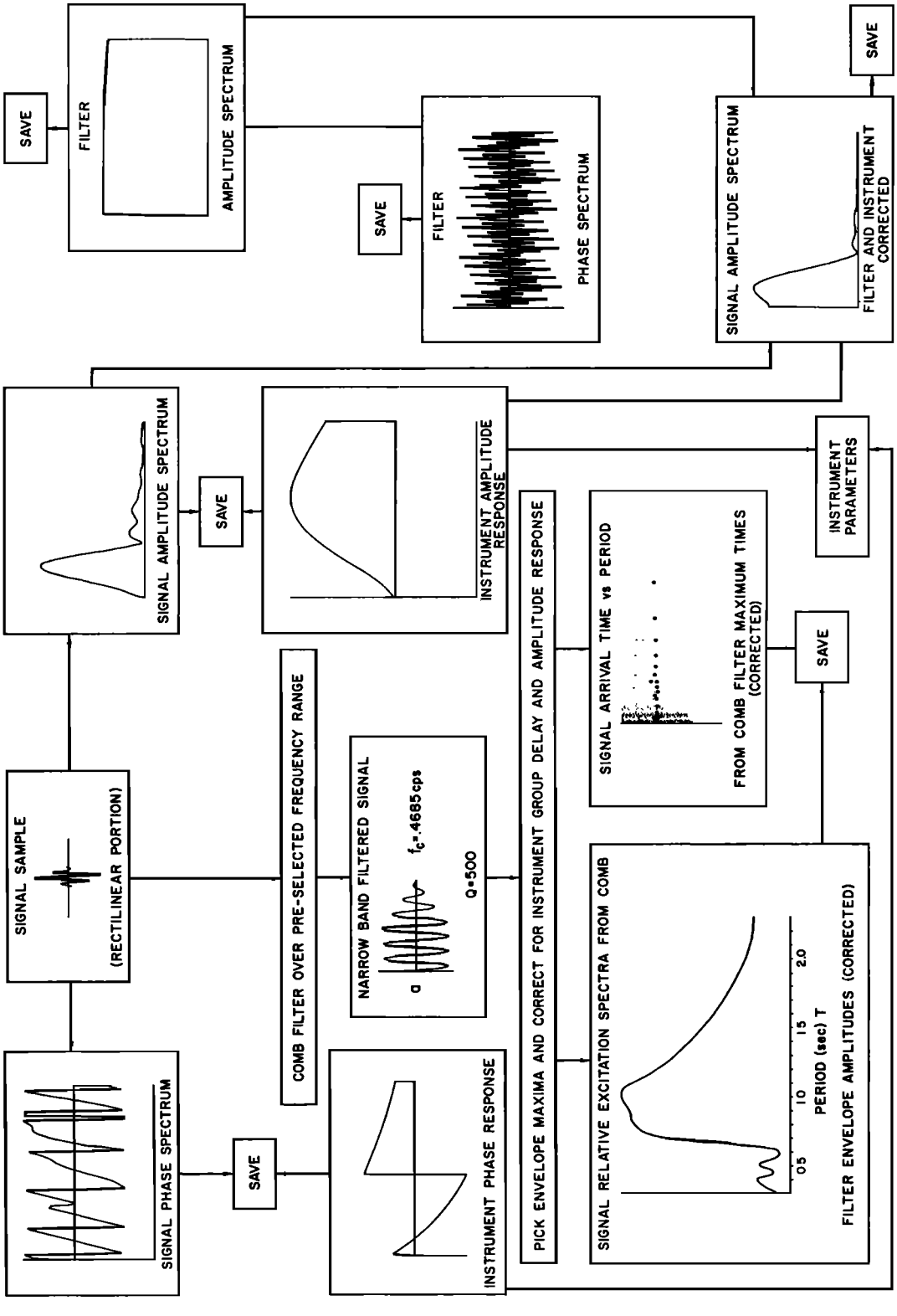

Fig. 5. Seismic wave analysis program (SWAP-9) *Section B*, amplitude and phase spectrums. Signal dispersion and relative excitation spectrums (comb filter processing).

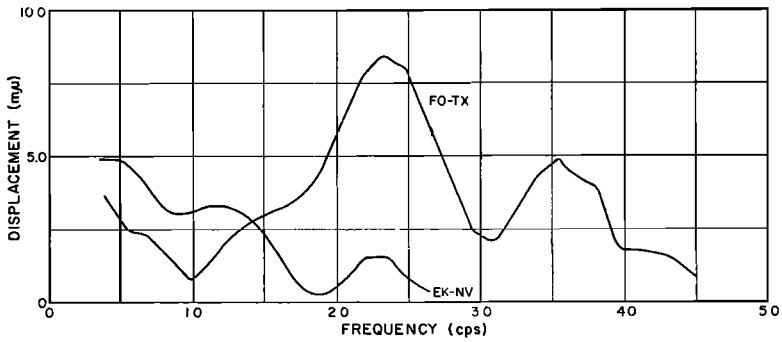

Fig. 6. P wave amplitude spectrums, station FO-TX, $\Delta = 1253$ km; and P wave amplitude spectrums, station EK-NV, $\Delta = 2533$ km (P_2 branch of travel-time curve) Salmon event.

points in the time-frequency plane, and the maximums of these arrivals at a given frequency are circled. As this illustration shows, the body phase dispersion is very small, as expected, and this has been consistently observed. The spectrums obtained from the envelope maximums therefore satisfy the criterion that they represent energy arriving with the expected (and predicted) small dispersion.

Interpretation of P Wave Amplitude Spectrums and Travel Times

Figures 6 and 7 show examples of the P wave spectrums at a few distances along the northwest profile. The spectrums have been corrected for instrument response and should provide an accurate estimate of the direct P wave ground displacement with minimum contamination from reverberation effects. The change in spectrums of the examples shown is due, in part, to differences in wave type—that is, P_n compared with P—as well as from distance effects on the amplitudes. In particular, Figure 6 shows P_n spectrums at a distance range where P_n is yet the first arrival, whereas other examples correspond to direct P arrivals. It is clear that the maximum amplitude for P waves shifts to longer periods with increasing distance because of the roughly linear increase in attenuation with frequency. The observed attenuation will, of course, be affected by the variation of the dissipation function with depth in the earth [e.g., *Anderson and Archambeau,* 1964], so that the attenuation will be dependent on the actual minimum time path followed by the phase. This effect would be of second order, however, compared with the much larger amplitude effects associated with the velocity variations with depth, particularly with velocity reversals and rapid or discontinuous changes in velocity.

A comparison of amplitude with distance at particular frequencies is given in Figure 8. The anomalous behavior only suggested by the individual spectrums is now quite apparent. The essential aspects of the amplitude-distance variation obtained and illustrated in this figure have been observed many times before by other investigators—in particular, for events observed along a profile of stations in this same region [e.g., *Romney et al.,* 1962]. The spectral detail in the present case may be somewhat greater than has been available before, and so a correspondingly more detailed interpretation will be advanced.

The spectrums will be interpreted together with the observed travel-time curves. However, viewed independently, they show a fairly rapid fall-off with distance out to approximately 1250 km. The rather gradual increase in amplitude, beginning at this point and reaching an apparent maximum at 1800 to 1900 km, probably indicates a first-arrival P phase that is different from P_n. The decrease in amplitude near 2000 km, followed by a second peak in the spectrum, probably indicates a second P phase.

This interpretation can be checked with the travel-time observations for evidence of discontinuous changes in the slope of the first-arrival curve, as well as for the existence of multiplicities or cusps in the curves accounting for the amplitude maximums.

Figure 9 shows the travel-time versus dis-

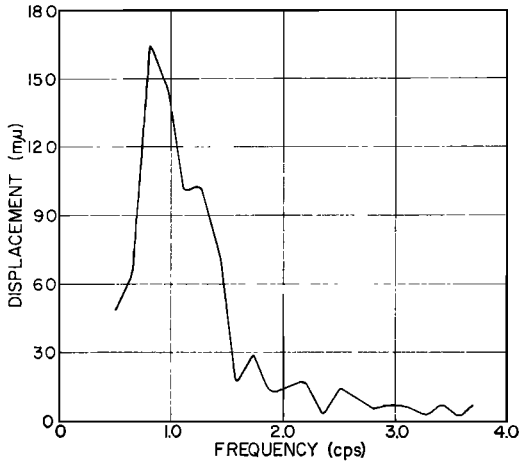

Fig. 7. P wave amplitude spectrums, station NL-AZ, $\Delta = 1927$ km, Salmon event (P_2 branch of travel-time curve).

tance data for the northwest profile; Figure 10 shows the data for the combined north and northeast profiles. Figure 11 shows the data for all profiles combined. These data correspond to first-arrival phases and all phases within 20 sec of the first arrival at a given distance, with the exception of those identified as *PP* and *PPP*. At the greater distances very late arrivals are shown because they were often of large amplitude and can be related to mantle velocity variations which manifest themselves in the first-arrival curve at somewhat greater distances. Figure 12 shows the travel times obtained for *PP* and *PPP* from the Remode processed time series. They have the expected character as functions of distance and serve, in part, to increase our confidence in the interpretation of travel times for P_n and P phases.

Some illustrations of the correlation process used in selecting and interpreting the P phases from the processed and original records are provided in Figure 13. The examples were chosen to show the first- and later-arrival P phases at several critical distances. The records are aligned along the times of first motion, and these times were chosen mainly on the basis of the original unfiltered records. The WF-MN station on the north profile is located at a distance appropriate to the simultaneous arrival of P_n and the phase P_1. Although the presence of two arrivals is not obvious from the records, there is some evidence for two distinct phases in both the processed and original time series, which is then supported by two corresponding recorded phases at nearer stations. The later phases on this record are all questionable and relatively small. The phase P_1 is included only to indicate the time of arrival for the retrograde branch of the direct P phase. This phase is either absent or very weak.

The P_1 phase on the RT-NM records is weak and is inferred primarily from the unfiltered trace; the remaining unquestioned phases are well defined on the filtered trace and can be correlated with the original time series. Here the retrograde phase P'_1 is relatively large.

The DR-CO filtered record is one of the better examples of phase isolation by the Remode process. However, as in almost every case, the initial P motion is very small. As previously suggested, this could be due to the relatively low S/N ratio for the initial motion. In any case, the first motion from the event can be selected on the basis of the original trace. The P_2 phase corresponds to one branch of the triplication in the travel-time curve, the P_1 phase continues to form the other, and P'_2 represents the late third arrival corresponding to the branch connecting P_1 and P_2. The large amplitudes associated with P_2 and P'_2 near the cusp in the travel-time curve are indicated by this filtered record. The three remaining stations are interpreted in a similar manner.

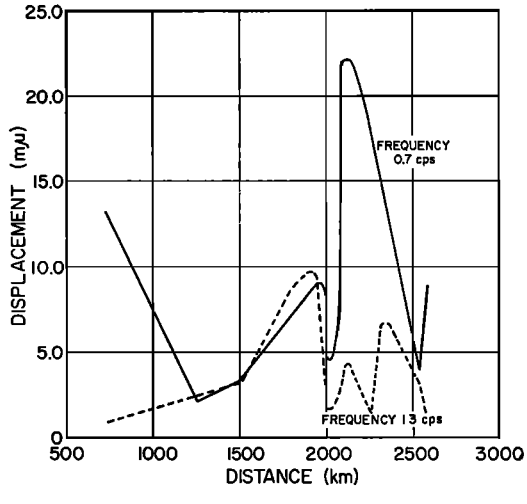

Fig. 8. Amplitude versus distance at fixed frequencies, northwest profile.

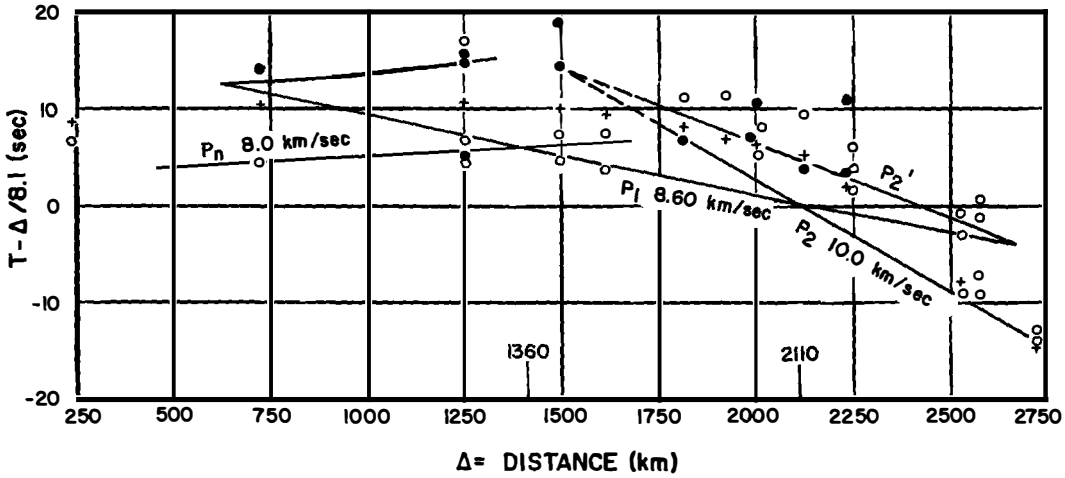

Fig. 9. Travel times versus distance, northwest profile, Salmon event. Solid circles indicate large amplitudes, open circles relatively small or moderate amplitudes, and crosses Jeffreys-Bullen travel times.

The travel-time curves drawn through the data points are based on the travel-time data themselves and on the previously discussed amplitude-distance spectrums. The curves also correspond in their general characteristics to theoretical curves obtained from the velocity structure shown in Figure 14. The initial selection of this structure was based upon a consideration of the long-period surface wave dispersion data obtained by a number of investigators and compiled by *Anderson and Toksöz* [1963]. The velocity structure in the mantle is a modified version of the CIT 11 oceanic model proposed by Anderson and Toksöz to explain the Love wave dispersion data. The model has also been found to provide good agreement between amplitudes and travel times from independent body wave data (D. L. Anderson, personal communication).

The only extensive modification to their structure is the addition of a crustal section and conversion to compressional velocities, which

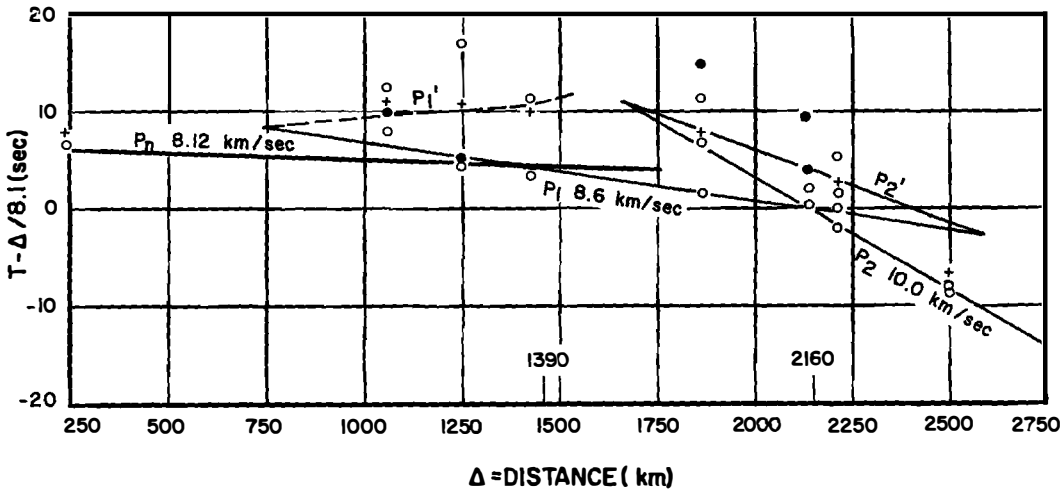

Fig. 10. Travel times versus distance, combined north and northeast profiles, Salmon event. Solid circles indicate large amplitudes, open circles relatively small or moderate amplitudes, and crosses Jeffreys-Bullen travel times.

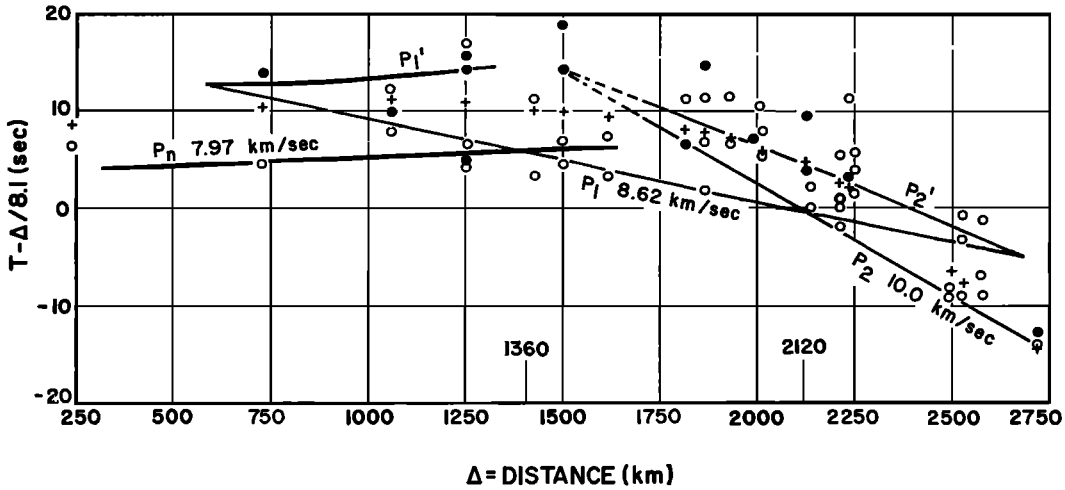

Fig. 11. Travel times versus distance, all profiles combined, Salmon event. Solid circles indicate large amplitudes, open circles relatively small or moderate amplitudes, and crosses Jeffreys-Bullen travel times.

involves assumptions of Poisson's ratio. Thus, in view of the essential agreement between continental and oceanic dispersion for periods beyond about 50 sec, the model agrees with continental long-period surface wave dispersion.

Although the structure has been checked and perturbed somewhat for consistency with the observed P phases, no particular effort has been made to adjust the fit to the P_n and other body phase data except in an approximate manner. For this reason, the structure shown should be regarded as a preliminary fit, which must be adjusted to account more fully for P_n, the reflected P phases, and the finer details of the direct P phases. The crustal section used here also corresponds to an average crust, which, for a finer fit, would have to be replaced by the crustal section appropriate to the particular region or regions involved in the travel-time profile. Initial models of the crust and upper mantle would come from the inversion of the shorter-period (10 to 50 sec) surface wave dispersion data. These data will be considered in a separate study.

A perturbation theory for the inversion of body wave data of the kind obtained in the

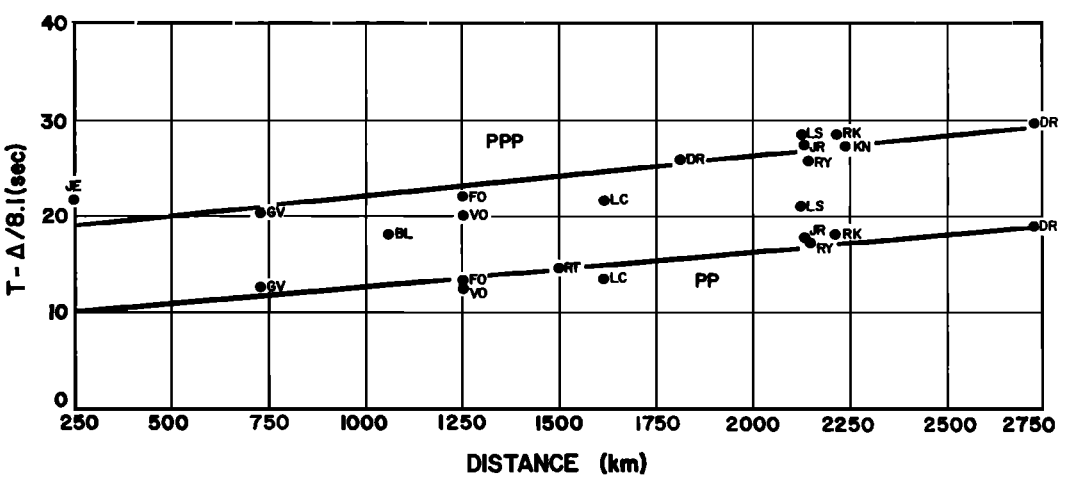

Fig. 12. Travel times for *PP* and *PPP* on all profiles, Salmon event.

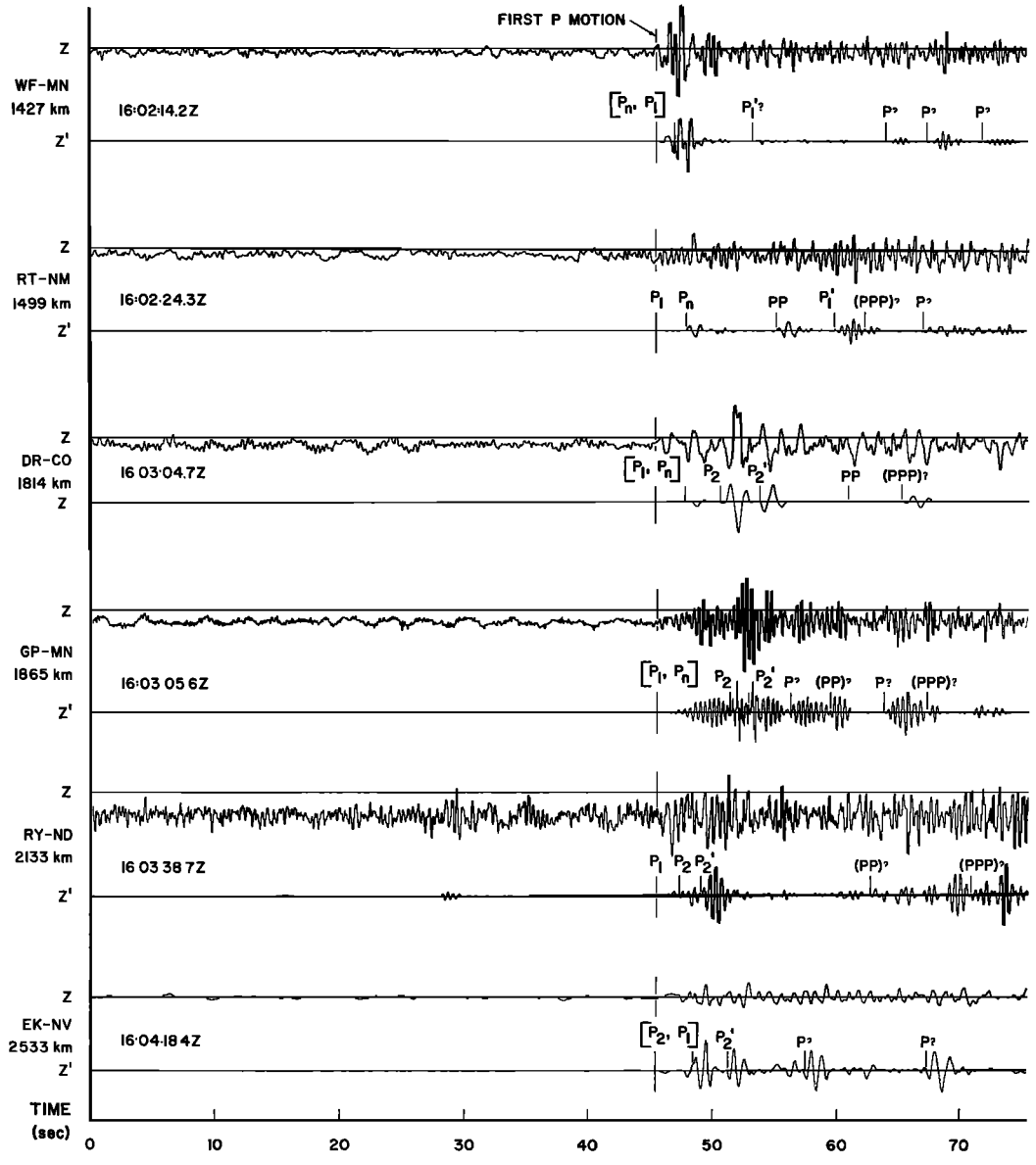

Fig. 13. Examples of processed records showing P phase selection at some critical distances.

present study is described by *Archambeau and Flinn* [1966]. In the present study the procedure was used only as an aid in modifying the structure because the inversion coefficients derived theoretically in the latter study predicted the way in which the structure should be modified for a better fit to the observations. Nevertheless, a fairly consistent explanation of all observations emerges from a comparison of the travel-time data with the amplitude-distance spectrums and the structure. In particular, the northwest-profile travel times (Figure 9) indicate a retrograde branch beginning at about 1500 km and extending back to a cusp near 750 km, where a forward branch of the curve begins (P_1) and eventually intersects the P_n curve. This multiplicity in the P curve is due to the low-velocity zone indicated in Figure 14,

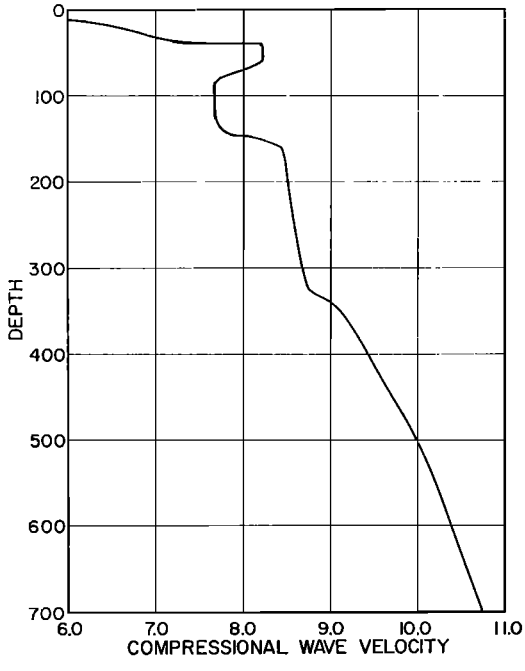

Fig. 14. Preliminary compressional velocity structure appropriate to travel-time observations, Salmon event.

the location of the cusp being controlled, primarily, by the steep velocity increase beginning at about 130 km. Theoretically one would expect large amplitudes in the neighborhood of the cusp, diminishing rather rapidly with increasing distance along the travel-time curve on the forward branch, and this is indicated by the relative amplitudes observed and shown on the travel-time curves. The intersection of the P_n and P_1 curves at approximately 1300 km seems well defined by the double arrivals corresponding to P_n and P_1 at the GV, FO, RT, and LC stations. The amplitude-distance spectrums also show a marked increase in amplitude of the first arrivals near 1300 km.

At distances less than 1300 km, P_n is the first arrival, and the amplitude-distance spectrums indicate a rapid fall-off with distance for the P_n energy at 0.7 cps. On the other hand, the energy at higher frequencies, although lower in amplitude, shows no such large slope. This would seem to delimit the thickness of the upper mantle high-velocity lid between the low-velocity zone and the M discontinuity, since the longer-period energy could be considered to leak into the low-velocity zone whereas that at shorter periods would not be nearly so much affected. However, the amplitude-distance spectrums in the epicentral range in question do not provide a dense enough distance coverage to enable us to draw very definite conclusions. The extension of P_n to 1300 km, and beyond that to at least 1600 km as a second arrival, must imply a fairly thick high-velocity region above the low-velocity zone, as was pointed out by *Lehmann* [1964]; otherwise P_n would attenuate far too rapidly with distance to be observed even by a sensitive filter technique. In the extreme case, P_n could not exist at all. In view of the present data, this mantle high-velocity section need not be extremely thick, of the order of 15 km [*Lehmann*, 1964], but it is probably thicker than is indicated in Figure 14.

Beyond 1300 km, P_1 is the first arrival and is definitely observed out to about 1600 km on the northwest profile, with P_n as a second arrival. At greater distances, P_1 arrivals are not detected on this profile, and the arrivals on the branch indicated as P_2 are the apparent first arrivals. However, the P_2 arrivals in the region of the cusp at 1700 km have large amplitudes, and P_1 should be relatively small. It is quite possible that the P_1 signals were weak enough in comparison with the noise and near enough in time to the large P_2 arrivals to be undetected either by visual or Remode processing. Hence the presence of P_1 beyond 1600 km can only be inferred. On the north profile in Figure 10, however, an arrival at station GP, at 1865 km, corresponds to P_1. The consistency of this arrival with all other P_1 arrivals is shown in Figure 11, where the data from all profiles are combined. Although at least one other interpretation is possible, it appears that reasonably good evidence exists for the presence of this P_1 branch and its extension out to approximately 2200 km as a first arrival. In addition, although the P_1 amplitudes would be large near the cusp because of the low-velocity zone, the amplitudes would be expected to fall off quite rapidly with distance.

The second multiplicity in the P wave travel-time curve, having P_2 as its forward branch, is due to a rapid increase in the velocity gradient and can be accounted for in terms of the marked velocity increase near a depth of 330 km in Figure 14. The observed travel times suggest

that the multiplicity is a triplication, the P_1 branch joining the retrograde P_2 branch to form a cusp. The forward cusp has very large amplitudes associated with it and is undoubtedly a caustic. Although the only direct evidence is the relative amplitude estimates for the arrivals at the relevant stations, it appears that the more distant cusp is also a caustic. This implies that the variation of the velocity gradient and the velocity itself are both continuous, since otherwise both cusps could not be caustics. Such a conclusion, however, is only tentative in view of the need for many more observations of both travel time and amplitude and the lack of detailed estimates of spectrums for the later arrivals near the more distant cusp. If the second cusp is not a caustic, the velocity gradient changes discontinuously at a depth near 330 km rather than continuously. On the other hand, if neither cusp was a caustic, a discontinuous jump in velocity would be implied [*Bullen*, 1961]. In view of the amplitude-distance spectral peak in the zone near the forward cusp, this latter velocity structure seems unlikely.

The details of the amplitude-distance spectrums in Figure 8 can be interpreted in a manner quite consistent with the previous interpretation of travel times. Thus the increase in amplitude at 1300 km is due to the emergence of the P_1 branch as the first arrival, but the continued rise to the point at 1800 km is associated with P_2. Therefore, the implied maximum in P_1 is only apparent, since P_2 was picked as the first arrival instead of P_1. The actual first arrival, P_1, undoubtedly has a low amplitude at this distance and would in any event have its largest amplitude where first measured near 1300 km. The shift toward shorter distances of the amplitude maximum associated with the cusp of the P_2 branch on the higher-frequency curve (1.3 cps) again indicates the frequency dependence of absorption in the earth. That is, the attenuation of the higher frequencies with distance of propagation is large enough to cause the maximum in this first-arrival amplitude curve to appear to rise very sharply and then to decrease rapidly with distance. Of course, the amplitude-distance curve plotted only for P_2 would have its maximum at the cusp near 1500 km. The spectrum of Figure 8 then shows that the higher frequencies fall off with distance away from the cusp at a much greater rate than the lower frequencies; this effect is due to absorption. The net effect, when only first arrivals are considered, is to produce a jump in the amplitude curve at the transition from P_1 to P_2. For high frequencies the curve for amplitude versus distance for first arrivals should then fall off rapidly, producing a clear maximum at the transition. For lower frequencies the maximum should appear at the transition, but it should be much less conspicuous (i.e., broader) because the attenuation with distance is much smaller. Figure 8 shows this effect, the transition occurring at about 2200 km.

Both the amplitude-distance curves in Figure 8 show a minimum at 2000 km which cannot readily be explained on the basis of the present interpretation of the data. It is possible that P_1 is late at the station involved and has been used for the spectral estimate, although it would have to be as much as 3 sec late. Alternatively, the observed minimum could be due to a station effect or an instrumental effect. The question cannot be resolved without more data.

The possibility that P_1 is late at distances beyond about 1700 km on the northwest profile does, however, suggest that P_1 is present and was detected beyond 1600 km but that the whole P_1 curve was shifted by about 3 sec to later times. The delay could then be attributed to a crustal thickening under the Rocky Mountains and a simultaneous deepening and extension of the low-velocity zone. Again, more data are necessary in order to test the hypothesis.

Such considerations naturally bring us to a comparison of the observations between the profiles. Since the north profile coverage was so sparse, it was combined with the northeast profile. Even so, the total number of stations used was small, so that conclusions concerning structure and the very nature of the travel-time curves are much more tentative than for the previous profile.

In general, the north-northeast profile appears to be similar to the northwest profile. There are, however, several differences that can be summarized as follows:

1. The P_n velocity is slightly higher on the north-northeast profile than on the northwest profile.

2. The duplication in the travel-time curve associated with the low-velocity zone is not so well defined, and it appears to be less pronounced. This would imply a smaller velocity decrease and a shallower bottom to the low-velocity zone. A similar conclusion is also suggested by the surface wave dispersion data obtained.

3. Observations of P_1 out to 1900 km, and again on either side of the transition to P_2 at 2165 km, indicate that P_1 can be detected over its entire range of existence. They also suggest either that the amplitudes of P_1 along the northwest profile were relatively small or that the P_1 times were all delayed beyond about 1600 km from the source. In either case, structural differences beginning at the bottom of the low-velocity zone are implied.

4. The triplication in the travel-time curve is quite well defined and does not differ significantly from that observed for the northwest profile.

Average travel-time curves for all profiles are given in Figure 11. The figure also shows the consistency of the phases isolated by the special filter used in this study.

Comparison of the travel times with the Jeffreys-Bullen (J-B) travel times for all profiles and stations shows that the J-B times are averages between the two arrivals in the region of the P wave duplication. They are consequently late compared with P_1. They also represent averages for the two branches of P_2 on the triplication. Thus P_1 appears to be ignored, and when present with sufficient amplitude or when not too close in time to the P_2 arrivals, as is the case on the north and northeast profiles, P_1 will provide early first-arrival observations. This, of course, is the case on the north and northeast profiles, but in the west, P_1 is late or has small amplitude, or both, so that the J-B times tend to agree quite closely with the observed first-arrival times. In all cases the J-B times agree closely with the travel-time curves given here for regions where the curves are single valued.

Inference of Source Properties and Structure from Body Wave Radiation Patterns

The amplitude spectrums discussed in the preceding section may also be used in estimating the symmetry of the source radiation pattern. Ideally, spectrums of P_2, P_1, and P_n should be obtained over their entire range of observation. In this way, a greater distance range could be covered for each phase.

In this preliminary study of the radiation patterns, only first arrivals are used, and the P_n and P data (P_1 and P_2 phases) are combined. However, it is easy to envision the separate P and P_n patterns from the contour diagrams given.

Figure 15 shows the radiation pattern in the

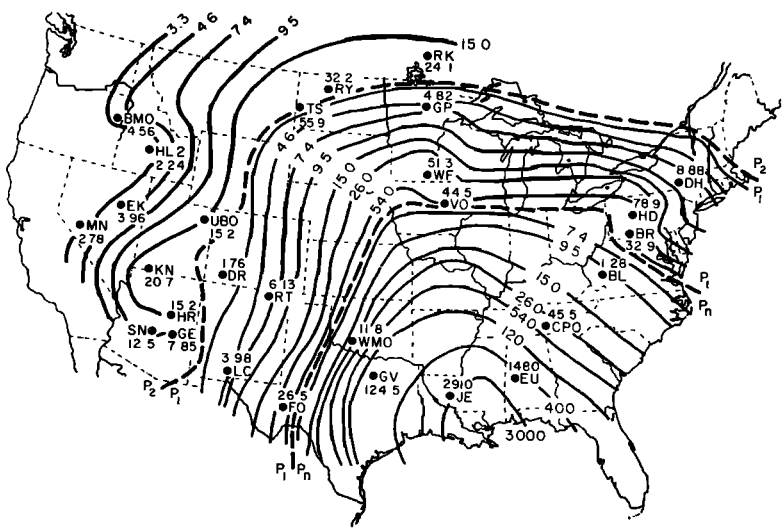

Fig. 15. Radiation patterns for P_n, P_1, and P_2 phases.

form of an amplitude contour diagram for the combined P_n and P data. The contour intervals are based on a $1/R^3$ scale for convenience. The P_1 arrivals are separated from the P_n arrivals on the basis of amplitude only. The division lines between P_n and P_1 and between P_1 and P_2 correspond to amplitude jumps and are found to agree reasonably well with the intersections of the P_n, P_1, and P_2 travel-time curves. The western part of the P_1-P_2 intersection is somewhat contorted and uncertain, again because of uncertainties in the identification of the phases.

The pattern for P_2 is considerably more irregular than for either P_n or P_1. The lack of good control and the preponderance of stations close to the line of discontinuity with P_1, particularly for the Arizona stations, are probable causes of variance in the pattern. In addition, noise contamination at the extreme distances is probably large enough to affect the amplitude estimates appreciably.

Nevertheless, taken together, the individual patterns are remarkably regular and show a strong circular symmetry about the source. There can be little doubt that the source, as viewed in terms of the seismic field at moderate distances, radiated compressional wave energy as an idealized explosive source. This conclusion is supported by the absence of Love wave excitation and also by the observed circular symmetry of the Rayleigh wave radiation in Figure 16.

The surface wave pattern shown in Figure 16 has been smoothed so that amplitudes at a few particular stations, which would give rise to strong local variations in the pattern, have been omitted. The expected result of this smoothing operation is a regional variation corresponding to the source pattern, with the effects of local variations of the near-surface velocity structure filtered out. These local structural effects would be expected to be large, and the smoothed radiation pattern must be interpreted with some degree of caution. The patterns obtained at several frequencies did, however, show consistent regional radiation patterns. The pattern shown in Figure 16 is typical of these observations, and we conclude that it is representative of the source Rayleigh wave field at this frequency, modified only by the regional changes in crust and upper mantle structure.

The actual departure from ideal circular symmetry of the Rayleigh wave radiation takes the form of a general shift of the pattern to the east. The travel times for P_1 and P_n are early in this zone, and, as other investigators have noted, early arrival times are correlated with large amplitudes. This correlation can be explained in terms of higher relative velocities, higher Q within the low-velocity zone, and a shallower bottom of the low-velocity zone to the east and north of the Salmon site. This explanation is consistent with the hypothesis dis-

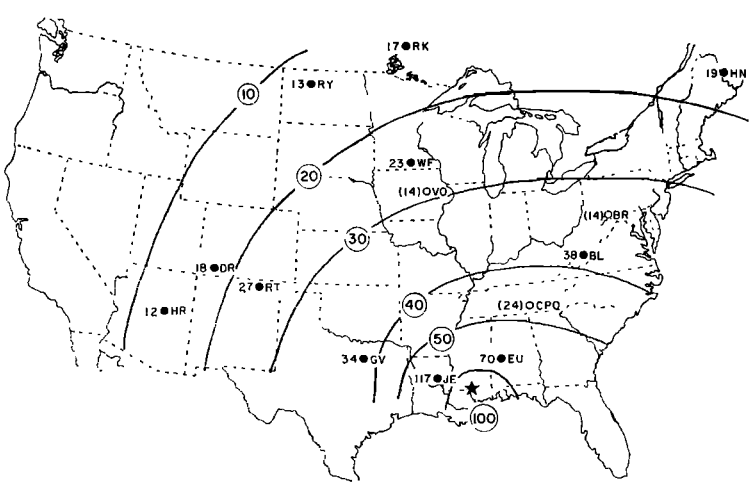

Fig. 16. Rayleigh wave radiation pattern at $T = 15$ sec, amplitude of vertical-component Rayleigh wave (in millimicrons) as a function of distance and azimuth, Salmon event.

cussed above, concerning delay in the P_1 travel time in the Rocky Mountain region.

Although circular symmetry for an explosive source is to be expected in theory, compressional and surface wave radiation patterns can and usually do depart from such symmetry. Specifically, regional and local variations of structure, strong structural anisotropy or inhomogeneity in the source region, or tectonic release can contribute to strong variations in symmetry and amplitude.

Tectonic release has, for many of the past NTS explosions, been suspected of contributing the major part of the anomalous shear wave radiation [*Press and Archambeau,* 1962; *Toksöz et al.,* 1964; *Archambeau,* 1964]. Figure 17 shows the theoretical dilatation and rotation amplitude patterns to be expected from an explosion in a prestressed medium [*Archambeau,* 1964]. These particular patterns result from a pure shear prestressed field, and the total dilatation field is given by the superposition of the spherically symmetric dilatation due to the explosion and the quadrupole part due to tectonic release. The rotational part of the field is anomalous in that it is due, in total, to tectonic release. The total energy in the tectonic radiation field is about equivalent to that expected from an event of magnitude 4.5 Thus, noting that the dilatation amplitudes are an order of magnitude less than the largest rotational component, we expect a 10% perturbation in the explosive dilatation field. On the other hand, the Love wave radiation would be due entirely to tectonic release, and the Rayleigh wave radiation would have a 50% or more variation due to tectonic release.

A small change in the compressional field, in the manner indicated in Figure 17, could probably not be detected in the P wave data from

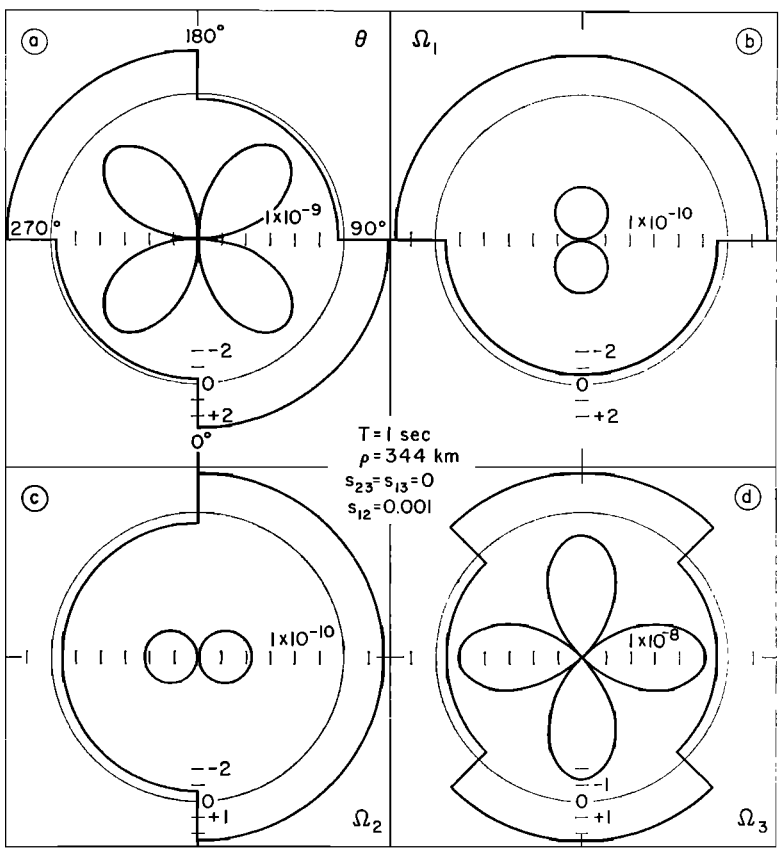

Fig. 17. Theoretical radiation patterns for P and S wave radiation due to shock-induced tectonic energy release.

Salmon. On the other hand, the absence of Love waves and the symmetry of the Rayleigh wave pattern in Figure 16 indicate little or no tectonic release, inasmuch as large effects would be expected. In addition, both the Rayleigh wave and body wave data show the same shift in pattern to the east, strongly implying a regional structural variation as the source of the effect.

Thus the *P* wave radiation pattern would not normally be expected to show the effects of tectonic release. In view of the surface wave evidence, however, it seems unlikely that tectonic release of any magnitude occurred with the Salmon event and that all perturbations in the amplitudes of the body phases are associated with regional structural variations.

In addition to the evidence from the teleseimic radiation field, the near-source field shows the spherical symmetry to be expected from a purely compressional point source [*Springer*, 1966]. In view of the agreement between the near- and far-field observations, we conclude that near-source inhomogeneities, which could scatter the primary energy from the source into anomalous *SH* radiation, for example, were absent or at least not strong enough to result in any appreciable energy conversion. In addition, the near-source observations of the first-motion compressional field, by themselves, suggest the absence of any tectonic release. However, as was previously pointed out, variation in the direct *P* wave field due to tectonic release would probably be small, so that observations of the shear field would also be necessary in order to conclude, definitely, that tectonic release did not occur.

Discussion and Conclusions

The principal practical difficulty in studies of this nature has been with the isolation or separation of body phases from noise and undesired signal. To some extent, the special filter used here has reduced this difficulty, but it is still necessary to correlate the filtered output with the original time series in order to select distinct body phases. The time information provided by the filtered seismograms—that is, the time of arrival of a given phase and the duration of the rectilinear motion—was also used as input to an automated spectrum analysis program, which then gave amplitude data for the body phases. The whole analysis process provided considerable information concerning the distant *P* wave field and is considered quite reliable when used with the original time series data.

The amplitude-time information was interpreted in terms of the source properties and the elastic properties of the medium. In particular, the lack of Love wave radiation, the symmetry of the Rayleigh wave radiation, and, from independent work by Springer and W. R. Hurdlow [*Springer*, 1966], the near-field first-arrival *P* wave symmetry all indicate a seismic source mechanism corresponding to a compressional point source. As such, the source is ideal for the interpretation of the travel times and amplitude spectrums of *P* phases, since source effects do not seriously complicate the interpretation in terms of structure. Thus the variation of *P* wave amplitude with distance and azimuth is interpreted in terms of the structural characteristics of the medium and may be correlated with the travel-time data.

The principal result of the study has been the interpretation of the travel-time and amplitude observations of the *P* wave arrivals in terms of regional structure. This explanation is, however, predicated on a proper interpretation of the discrete set of amplitude-time observations. In this regard, the travel-time data, by themselves, suggest discontinuous breaks in the first-arrival travel-time curve at distances of about 1350 and 2200 km from the source, and the observed later-arrival phases can be interpreted in a manner consistent with the interpretation of the first arrivals. The interpretation is supported by the amplitude observations which independently show a discontinuous change in the amplitude-distance curve for first arrivals at 1350 and 2200 km. In addition, the secondary arrivals near the cusps in the inferred travel-time curve show relatively large amplitudes, as would be expected. These amplitude properties are also correlated in azimuth around the source. Thus a consistent interpretation of both the amplitudes and travel times of the phases is provided by the inferred travel-time curve.

Finally, the body wave data as described by this travel time curve can be associated with a velocity structure which is in essential agree-

ment with observations of surface wave dispersion.

The structure implied by the data along north and northeast profiles from the source indicates a weak low-velocity zone, or possibly its total absence. This is in contrast to the western profile, where the low-velocity zone is well defined and is terminated by a rapid velocity increase at a depth near 130 km. This low-velocity zone and the continuous and rapid velocity increase at 130 km account for the duplication in the travel-time curve in the near-distance range.

The structures for both regions show a second strong velocity increase near a depth of 330 km which is probably continuous. This feature accounts for the triplication in the travel-time curves. The time data from the west profile appear to be delayed in the distance range beyond about 1700 km in comparison with the data for nearer distances and with the data from the east profiles. The effect is probably due to a thickening of the crust and an extension of the low-velocity zone under the Rocky Mountains.

Finally, it is observed that the J-B travel times tend to correspond to averages of the first and second arrivals at distances where there is a duplication or triplication in the travel-time curve, the averages being weighted toward the larger-amplitude arrivals.

Note added in proof. Recent work on travel times from NTS explosions by D. G. Lambert (to be published) shows that we can eliminate many of the points that scatter away from the interpolated travel-time curves in Figures 9, 10, and 11. The technique is to compute a synthetic seismogram (including *P-S* conversions) for an assumed crust in the vicinity of the source. Later arrivals at teleseismic distances are eliminated on the basis of correspondence in relative arrival time *and relative amplitude* to multiples of earlier arrivals. Although the method is partly subjective, more than half of the later arrivals can be confidently identified as near-source multiples. The remaining arrivals considerably strengthen interpretation of the data in terms of a multiple-branched time-distance function.

Acknowledgments. This research was supported by the U. S. Atomic Energy Commission in cooperation with the Advanced Research Projects Agency, Nuclear Test Detection Office, and was monitored by the Air Force Technical Applications Center under contract AF 33(657)-12447.

References

Anderson, D. L., and C. B. Archambeau, The anelasticity of the earth, *J. Geophys. Res., 69,* 2071–2084, 1964.

Anderson, D. L., and M. N. Toksöz, Surface waves on a spherical earth, 1, Upper mantle structure from love waves, *J. Geophys. Res., 68,* 3483–3499, 1963.

Archambeau, C. B., Elastodynamic source theory, Ph.D. thesis, California Institute of Technology, Pasadena, 1964.

Archambeau, C. B., and E. A. Flinn, Detection, analysis, and interpretation of the teleseismic signal from the Salmon event, *Seismic Data Lab. Rept. 120,* ARPA Order 624, 1965.

Archambeau, C. B., and E. A. Flinn, Perturbation theory for the inversion of body wave travel-time data, *Seismic Data Lab. Rept.,* ARPA Order 624, AF33(657)-15919, April 1966.

Bullen, K. E., A new method of deriving seismic velocity distribution from travel-time data, *Geophys. J., 3,* 258–269, 1960.

Bullen, K. E., Seismic ray theory, *Geophys. J., 4,* 93–105, 1961.

Kovach, R. L., and D. L. Anderson, Long-period Love waves in a heterogeneous spherical earth, *J. Geophys. Res.,* 67, 5243–5244, 1962.

Lehmann, I., On the travel times of *P* as determined from nuclear explosions, *Bull. Seismol. Soc. Am., 54,* 123–139, 1964.

Press, F., and C. B. Archambeau, Release of tectonic strain by underground nuclear explosions, *J. Geophys. Res., 67,* 337–343, 1962.

Romney, C., B. G. Brooks, R. H. Mansfield, D. S. Carder, J. N. Jordan, and D. W. Gordon, Travel times and amplitudes of principal body phases recorded from Gnome, *Bull. Seismol. Soc. Am., 52,* 1057–1074, 1962.

Sax, R. L., and C. H. Mims, Rectilinear motion detection, *Seismic Data Lab. Rept. 118,* ARPA Order 624, AF 33(657) 12447, March 1965.

Shimshoni, M., and S. W. Smith, Seismic signal enhancement with three-component detectors, *Geophysics, 24,* 664–671, 1964.

Springer, D. L., Calculation of first-zone P wave amplitudes for Salmon event and for decoupled sources, *J. Geophys. Res., 71*(14), 1966.

Toksöz, M. N., A. Ben-Menahem, and D. G. Harkrider, Determination of source parameters by amplitude equalization of seismic waves, 2, Release of strain by underground nuclear explosions, *J. Geophys. Res., 69,* 4355–4366, 1964.

(Manuscript received February 16, 1966; revised April 8, 1966.)